View metadata, citation and similar papers at core.ac.uk
brought to you by CORE
provided by Digital.CSIC

Theoretical and experimental characterization of TiO_2 thin films deposited at oblique angles

R Álvarez[1], L González-García[1], P Romero-Gómez[1], V Rico[1], J Cotrino[1,2], A R González-Elipe[1], A Palmero[1]

[1] Instituto de Ciencia de Materiales de Sevilla (CSIC - Universidad de Sevilla). Av. Américo Vespucio 49, 41092 Sevilla, Spain
[2] Departamento de Física Atómica, Molecular y Nuclear (Universidad de Sevilla). Av. Reina Mercedes, s/n, 41012 Sevilla, Spain

E-mail: rafael.alvarez@icmse.csic.es

Abstract. The microstructural features of amorphous TiO_2 thin films grown by the electron beam physical vapour deposition technique at oblique angles have been experimentally and theoretically studied. The microstructural features of the deposited films were characterized by considering both, the column tilt angle and the increase of the column thickness with height. A Monte Carlo model of the film growth has been developed that takes into account surface shadowing, short-range interaction between the deposition species and the film surface, as well as the angular broadening of the deposition flux when arriving at the substrate. The good match between simulations and experimental results indicates the importance of these factors in the growth and microstructural development of thin films deposited at oblique angles.

PACS: 81.15.Aa, 81.15.Jj, 68.55.-a

1. Introduction

Oblique angle deposition (OAD) is a well-known deposition technique devoted to engineer thin films with columnar microstructures. This particular morphology is of interest because it allows the optimization of the film surface area [1-2] and it may render anisotropic physical properties such as dichroism, birefringence, anisotropic resistivity, etc. [3-5]. In general, these microstructures are caused by the shadowing of the deposition flux when arriving at the growing film, which makes tall surface features prevent the deposition under their shadow. This produces a competitive growth among surface motives, which ends up in the development of tilted structures oriented towards the incoming deposition flux [6-19]. The use of these thin films as a host for the development of nanostructured composite materials is another potential application quite dependent on the final topology of the films that has been widely investigated by our group [20-23].

Among all possible magnitudes that define a columnar film microstructure, the relation between the column tilt angle, β, and the incident angle of the vapour flux, α, for non-rotating substrates, is of great relevance and has been the subject of intense debate in the literature in the last years. In ref. [24], for instance, Nieuwenhuizen and Haanstra proposed the well-known tangent rule

$$\tan\alpha = 2\tan\beta, \quad (1)$$

which was derived from experimental data rather than from basic principles. Eq.(1) describes adequately the relation between α and β for α<60º but provides a poor description otherwise. Tait et al. proposed the relation known as the cosine rule

$$\beta = \alpha - \arcsin\left(\frac{1-\cos\alpha}{2}\right), \quad (2)$$

which finds a better agreement for $\alpha > 60$º in some cases [25]. Other expressions relating α and β have been proposed in the literature aiming at a general description of the film growth, although such relationships depend on the film chemical composition and deposition conditions, and require some fitting parameters whose physical meaning is, in most of the cases, unclear [26]. In addition to this debate, there is also great interest in understanding the relation between the average column thickness, ξ, and the height, d. This accounts for the widening of the columns as their length increases: a phenomenon that has been reported in the literature and is responsible for a strong dependence of film properties on the film thickness [27-29].

Numerical models have provided further insight into the growing mechanisms leading to the formation of columnar structures, describing the relation between α and β, as well as between ξ and d [30-32]. In ref. [33] a three dimensional Monte Carlo (MC) model of the ballistic deposition was developed to understand the low temperature growth of oblique angle deposited thin films. In that reference, the directionality of the deposition flux together with the surface shadowing mechanism was found responsible for the formation and growth of columns. Moreover, to account for the importance of the substrate temperature and the diffusion rates, surface relaxation was introduced via thermal activation in a hopping mechanism with an Arrenius-type temperature dependence [30-32,34-35]. The influence of the film temperature, T, on the film growth was explained by the so-called Structure Zone Model (SZM) [36]. This model defines different types of growth depending on the value of the ratio T/T_m, being T_m the film melting point. For increasing values of T/T_m the growths are divided into three zones: i) Zone I, which corresponds to a low temperature growth and characterized by a dominant shadowing mechanism and a negligible adatom diffusion, ii) Zone T, where surface diffusion starts to play a role in the growth, and iii) Zone II, where surface and bulk diffusion influence the film nanostructure. A more complex description was carried out in ref. [37], where a "one-atom" molecular dynamic simulation accounted for the oblique-incidence growth of (100) oriented metals. Results indicated that the interaction between deposition species and the film surface is relevant for the control of the surface morphology, and therefore of the anisotropy and roughness of the simulated films. The quantitative description of the columnar growth of thin films by OAD, and, in particular, of the relevance of the interaction between a deposition particle and the film surface on the relation between α and β, has motivated this paper. Herein, we study the OAD of thin films from both theoretical and experimental points of view. With this purpose we have deposited amorphous TiO_2 thin films under different conditions and analyzed their microstructural features. This oxide has been employed as a test material due to its wide use in large number of applications [14-15,38-39], where a tight correlation between nanostructure and functional properties is determinant for its performance. On the other hand, we have developed a Monte Carlo (MC) model of the film growth that takes into account the short-range interaction between the film surface and the incoming deposition atoms, as well as the angular distribution of the deposition flux. We have found that the results of our model are in good agreement with our experiments and other data in the literature, and that they adequately reproduce the dependence of β on α, and that of ξ on d, in all the studied cases. Despite the fact that our model has only been tested for TiO_2 thin films, we think that it introduces general concepts and a reference framework applicable to the growth of other materials by OAD when film temperature is low enough to make shadowing the dominant growth mechanism (i.e., when film growth is in Zone I in the SZM).

This paper is organized as follows: in section 2 we describe the experimental setup, while the development of the model is described in section 3. In section 4 we present and discuss the obtained results and compare them with the model predictions. Finally, in section 5 we summarize the conclusions.

2. Experimental setup

Amorphous TiO_2 thin films were deposited by electron beam physical vapour deposition at oblique angles at room temperature on silicon substrates. Evaporation was carried out in an O_2 atmosphere at a pressure of 10^{-2} Pa by using TiO_2 pellets as target material. TiO_2 thin films were prepared by placing the substrates at different oblique angle geometries (from α = 60º to α = 85º) with respect to the evaporator source (Fig 1a). The layer thickness was controlled by monitoring the evaporation process with a quartz crystal monitor previously calibrated, finding that the deposition rate was 0.1 nm s^{-1}. Deposition times were set to obtain thin films with thicknesses around 500 nm. The microstructure of the films was examined by means of a field enhanced scanning electron microscope (FESEM), HITACHI S5200. Cross section views of the thin films were obtained by cleaving the samples deposited on silicon substrates.

3. Theoretical Model

Our MC growth model follows the formulation used in refs. [30,35,40-41]. We consider the deposition of effective particles on a cubic three-dimensional $N_L \times N_L \times N_H$ grid with periodic boundary conditions, whose cells may take the values 0 (empty cell), or 1. Two cubic grid cells that share a facet of their cubes are called nearest-neighbourgs (NN). Each deposition particle moves towards the substrate from an initial random position above the surface and along a direction defined by the spherical angles θ and φ, where $\theta \in [0,\pi/2)$ is the polar angle of incidence ($\theta = 0$ is the direction normal to the target) and $\varphi \in [0,2\pi)$ is the azimuthal angle. These angles are randomly selected according to the probability distribution density $P(\theta,\varphi)$, given by the relation $dP(\Omega) = d\Omega \int_0^{+\infty} d\mathrm{v}\, \mathrm{v}^2 F(\vec{\mathrm{v}})\, \vec{\mathrm{v}} \cdot \vec{s} \propto f(\theta,\varphi) \cos\theta \, d\Omega$, where $d\Omega = \sin(\theta) d\theta d\varphi$ is the diferential solid angle, $\vec{\mathrm{v}}$ is the velocity vector, v its modulus, $F(\vec{\mathrm{v}})$ the velocity distribution function of the deposition particles in the gas phase, and $\vec{s}$ a unit vector perpendicular to the deposition surface. If the particles were isotropically directed in the gas phase, we would have $f(\theta,\varphi)$=const., a case that we have studied in a previous publication [40]. In OAD, on the other hand, there is a well-defined preferential direction for the deposition particles, which makes us consider $f(\theta,\varphi)$ as a Gaussian distribution function centered on the main direction of the incident particle flux ($\theta=\alpha$, φ=0), with a variance σ. This takes into account the angular broadening of the flux of evaporated particles caused by the finite size of the source or by collisions in the gas phase. In this way, $f(\theta,\varphi) \propto \exp(-\theta_0^2/2\sigma^2)$, where the angles (θ_0,φ_0) are taken relative to the main incident direction, and are thus related to (θ,φ) by a rotation of the coordinate system, $\cos(\theta_0)=\cos(\theta)\cos(\alpha)+\sin(\theta)\sin(\alpha)\cos(\varphi)$ (see Fig.1b).

Particles follow linear trajectories until they are incorporated onto the film. From a physical point of view, each effective particle accounts for a Ti species that, after being deposited, instantaneously turns into a TiO_2 effective block in the material, occupying a cubic volume Δ^3. Consequently, we estimate the typical size of the blocks as the actual average distance between two Ti atoms in the amorphous network, i.e., $\Delta \sim$ 3–4 Å [42].

The incorporation of the deposition particles onto the film is known to strongly depend on the particular features of the interaction potential between the surface and the incident Ti particle. Thus, taking into account the spatial discretization we have carried out in our model, we consider three different interaction zones depending on the distance between deposition particle and film surface, which we call r: i) for $r \leq \Delta$, we consider the interaction strong enough to make the particle stick to the surface with probability 1, ii) when $\Delta < r \leq 2\Delta$, we consider that

the interacion has weaken, but there is still a chance for sticking, with a probability s_{nn}, and iii) for r > 2Δ we consider that the interaction is so weak that no sticking is possible. It is worthy to mention that the typical interaction distance we consider (Δ ~ 3–4 Å) is in the same order as that appearing in well known short-range interactions such as Van der Waals-type or Lennard-Jones-type potentials, for instance. The study of the particular relation between the interaction potential and the values of the sticking probabilities as a function of r, for typical relative velocities and impact parameters, is far from the scope of this paper. However, as we will see below, this simple approximation is enough to characterize the growth of the films and their microstructure.

The set of rules introduced in our MC model to account for the interaction between the deposition particle and the film surface is easily implemented as follows: i) when the deposition particle, in its movement towards the film surface, has a head-on collision with an already deposited particle (i.e., it tries to pass through an occupied cell), we consider that it always sticks with probability 1 and is deposited in the previous cell along its movement, ii) when the deposition particle passes next to an occupied nearest-neighbour (NN) cell along its trajectory, we consider that the particle sticks to that cell with a probability s_{nn}, iii) if none of the abovementioned rules are applicable, the particle keeps moving. The concept of NN sticking coefficient, s_{nn}, has been previously introduced in the literature by different authors in order to account for the short-range interaction between the deposition particle and the surface atoms, and in general it depends on the features of the interaction potential between the surface and the incoming particle, as well as on its kinetic energy and film temperature [43-45]. The importance of this coefficient in OAD can be seen in figure 1c, which shows how this mechanism may modify the columnar growth direction by incorporating more particles in the vertical direction, thus affecting the film morphology and tilt angle of the columns. In figure 2 we detail the main deposition rules applicable in our MC model, as well as the dependence of the sticking probability on the deposition particle/film surface distance.

The MC model can be solved as a function of three input parameters: α, σ and s_{nn}. We do not consider temperature-activated processes such as surface diffusion or particle desorption, since the typical threshold energy for these processes is in the order of 1 eV, and therefore they can be neglected given the low temperature of the films during growth. This approximation is in agreement with the low value of T/T_m in our experimental conditions for TiO_2, T/T_m~0.15. Moreover, the low energy of the deposition particles made us neglect any surface re-emission processes (in agreement with ref. [46]), whereas no Ehrlich-Schwoebel potential barrier has been considered, as there are not well-defined atomic steps on amorphous films [47].

4. Results and Discussion

4.1. Experimental thin film microstructure

Cross-sectional FESEM images of the TiO_2 thin films are shown in Fig. 3a-d for increasing values of α. Film microstructures are defined by columnar motives with different tilt angles and a column thickness that increases with height. In figure 4 we show the value of β as a function of α, together with other data found in the literature for low-temperature OAD of TiO_2 thin films [37,48]. As a general behaviour, β increases with the value of α, which agrees with the trends predicted by eq. (1) or eq. (2), although it seems clear that these two expressions overestimate the value of β in all the studied conditions.

By using standard techniques of image treatment, such as those employed in granulometry, we have been able to determine the average thickness of the columnar structures at a given height. In figure 5 we depict the relation between average column thickness ξ, measured from the FESEM images presented in figure 3, and height, d, for different values of α. As expected [29], column thickness grows as $\xi \sim d^p$, ranging the value of the growth exponent, p, between p =

0.16 ± 0.02 for $\alpha = 60°$ and $p = 0.64 \pm 0.02$ for $\alpha = 85°$.

4.2. Simulation results

The MC model described in section 3 has been solved for different values of α, σ and s_{nn}. The size of the three dimensional grid was taken as $N_L = 2500$ and $N_H = 1500$, which ensures that no finite size artifacts are present in the solutions. The microstructure of the simulated films always consisted of tilted columns whose diameters increased with the height. Figure 6 shows the simulated structures as a function of s_{nn} and σ for $\alpha = 80°$. In general, an increase of s_{nn} clearly affects β, diminishing its value. On the other hand, the value of σ has relevance on the widening of the columns for increasing height. The relation between α and the calculated value of β is depicted in figure 7 for different values of s_{nn} and σ. First remarkable result is that all the experimental values of β reported in figure 4 are within the range of those obtained by the MC model. Moreover, it is apparent that, given a value for s_{nn}, the calculated value of β depends very weakly on σ, as can be seen in figure 7, which can be understood by taking in consideration that σ does not influence the value of the mean incident angle of the deposition particles. Interestingly, β shows a strong dependence on the value of s_{nn}. Thus, the case s_{nn}=0 represents the solution of a typical ballistic deposition model (not including NN sticking procesess), and as soon as the value of s_{nn} increases, the curve shifts downwards, showing a significative decrease of the column angle even for s_{nn} values as low as $s_{nn} = 0.05$. This decrease in β can be understood by considering that particles deposited due to the interaction with nearest-neighbours at the film surface add a new growth vector perpendicular to the substrate (Fig. 1c).

In figure 8 we represent the value of the column thickness as a function of height for different values of σ, $\alpha = 80°$ and s_{nn}=0.12, which were chosen for convenience. Slices from the three dimensional grid, parallel to the substrate, were analyzed in order to calculate ξ as a function of d, in the cross section plane shown in figure 6. In figure 8 we show the calculation results for σ values ranging from 1° to 10° where we obtain again the relation $\xi \sim d^p$. More interesting is the obtained dependence of the exponent p with the angular width of the particle flux (parameter σ), which ranges from $p = 0.20 \pm 0.03$ for $\sigma = 1°$ to $p = 0.53 \pm 0.03$ for $\sigma = 10°$.

4.3. Comparison between model and experimental results

Under our experimental conditions, the value of α is well-known and can be used in each case as an input parameter in our model. On the other hand, the values of s_{nn} and σ are not known, and must be found through a fitting technique to the experimental data. Nevertheless, since these two quantities are associated to mechanisms that should not change throughout all our experimental conditions (i.e. target size, film material, chamber pressure, substrate temperature, average kinetic energy of the deposition particles, etc.), we only need one experimental case to perform the fit and check whether the model predicts adequately the rest of the experimental data. For this we have chosen the film deposited with $\alpha = 80°$, finding the best agreement for the values s_{nn}= 0.12 and $\sigma = 6°$ (as can be seen from figures 4 and 8).

The relation between α and β obtained through the simulations appears in figure 4, where we find that the values s_{nn}= 0.12 and $\sigma = 6°$ reproduce well our experimental data, not only for $\alpha =$ 80°, but for all the studied cases. In order to make more apparent the agreement between experimental data and the solutions of the model, in figures 3e-h (right column figures) we have included the cross-sectional images of the simulated microstructures, which can be compared with the corresponding experimental data in figures 3a-d (left column figures). Moreover, the dependence between ξ and d is depicted in figure 9. In this case, we again find a good agreement between the calculated values of p and the experimental ones in all the studied cases. This good agreement ensures that the values s_{nn}= 0.12 and $\sigma = 6°$ are adequate to reproduce and predict the most important features of the film microstructures, and therefore strongly indicates

that they are not merely two fitting parameters, but the effective representations of physical processes. We have to stress that this column thickness corresponds to the cross section plane shown in figure 3. The column width corresponding to a perpendicular cross sectional view is expected to be different, and is known to be responsible for column coalescence and appearance of fan-like structures [34]. The values of the corresponding exponents predicted by the model are $p_{\perp}(\alpha = 60º) = 0.42 \pm 0.03$, $p_{\perp}(\alpha = 70º) = 0.46 \pm 0.03$, $p_{\perp}(\alpha = 80º) = 0.56 \pm 0.03$, and $p_{\perp}(\alpha = 85º) = 0.60 \pm 0.03$.

A discussion on how the short-range interaction potential may lead to a value of $s_{nn}= 0.12$ in our model, or about the specific processes that made $\sigma = 6º$ in our deposition reactor, is far from the scope of this paper. Nevertheless, they are within the range of expected values; for instance, angular broadening should be few degrees as the size of the emission spot at the target is very small, and the background oxygen pressure is low enough to neglect scattering processes of the Ti species in the gas phase. Moreover, the NN sticking probability should also be low, as it would only account for atomic interactions in the range comprised between ~3 and 8 Å, where such interaction is weak, and the sticking probability should be far below 1. Nevertheless, we have shown the importance of taking into account these two processes in order to properly determine the film microstructure even when their values are as low as $s_{nn}= 0.12$ and $\sigma = 6º$.

The results of the model open a way for an enhanced control on the microstructural features of oblique angle deposited films via the experimental modification of σ. Larger particle sources or higher pressure values (that shorten the incident particle mean free path and thus enhance collisions) increase the value of σ and, in agreement with our model, the value of p. On the other hand, particle beam collimators or filters will reduce the value of p, hence producing thin columnar structures with low increase of column thickness with height. Finally, although the MC model has been developed regarding the OAD of TiO_2 thin films, our aim is general and we think it can be applicable to other OAD depositions within Zone I of the SZM.

5. Summary and Conclusions

We have performed both experimental and theoretical studies on the morphological features of TiO_2 thin films grown by oblique angle deposition. On one hand, we have experimentally carried out thin film depositions at room temperature for different values of the substrate tilt angle, α, and studied the resulting column tilt angle, β. This latter defines the microstructure of the material as experimentally determined through cross-section field emission scanning electron microscopy images. In addition, we have also characterized the increase of the column thickness, ξ, as a function of height, d. By means of a Monte Carlo model we have been able to characterize the growth and microstructural features of these films. This model takes into account the short-range interactions between the film and the deposition species as well as the broadening of the deposition flux. These two processes have been shown to govern the growth and the microstructural development of the TiO_2 studied films.

The validity of the model is restrained to the conditions where surface shadowing dominates the film growth and nanostructuring (Zone I in the SZM), i.e., whenever thermally activated processes are not relevant in the deposition, implying a low temperature deposition and when the incident deposition particles possess low kinetic energy (i.e. they do not bounce off after a collision with the film surface). Furthermore, the absence of potential barriers that simulate crystalline growth limits the use of this model to amorphous material. Finally, given the good agreement obtained for TiO_2, we expect this model to be applicable to the study of other OAD amorphous films grown whenever surface shadowing dominates the growth, and therefore to be used as a predictive tool in the growth of OAD films with a taylored morphology.

Acknowledgements.- R. Álvarez acknowledges the JAE program of the Spanish Council of Research (CSIC). Financial support from the Spanish Ministry of Innovation (projects MAT

2007-65764, CONSOLIDER INGENIO 2010-CSD2008-00023 and PIE 200960I132) and the Junta de Andalucía (projects TEP2275, TEP5283, P07-FQM-03298 and FQM-6900) is acknowledged.

References

[1] Robbie K and Brett M J 1997 *J. Vac. Sci. Technol.* A **15** 1460
[2] Suzuki M and Taga Y 2001 *J. Appl. Phys*. **90** 5599
[3] Lakhtakia A, McCall M W, Sherwin J A, Wu Q H and Hodgkinson I J 2001 *Opt. Commun*. **194** 33
[4] Mbise G, Smith G B, Niklasson G A and Granqvist G C 1989 *Appl. Phys. Lett*. **54** 987
[5] Hodgkinson I and Wu Q H 1999 *Appl. Opt*. **38** 3621
[6] Meakin P, *Fractals, Scaling and Growth Far from Equilibrium* (Cambridge University Press, New York, 1998)
[7] Pelliccione M and Lu T-M, *Evolution of Thin Film Morphology: Modeling and Simulations*, Springer Series in Materials Science Vol. 108 (Springer, New York, 2008)
[8] Barabási A L and Stanley H E, *Fractal Concepts in Surface Growth* (Cambridge University Press, Cambridge, 1995).
[9] Garcia-Martin J M, Alvarez R, Romero-Gomez P, Cebollada A and Palmero A 2010 *Appl. Phys. Lett*. **97** 173103
[10] Schubert E, Hoche T, Frost F, Rauschenbach B 2005 *Appl. Phys*. A **81** 481
[11] Zhao Y-P, Ye D-X, Wang G-C and Lu T-M 2002 *Nano Lett*. **2** 351
[12] Lintymer J, Martin N, Chappe J-M, Takadoum J 2008 *Wear* **264** 444
[13] Zhou C M and Gall D 2008 *J. Appl. Phys*. **103** 014307
[14] Kesapragada S V and Gall D 2006 *Thin Solid Films* **494** 234
[15] Kesapragada S V, Victor P, Nalamasu O and Gall D 2006 *Nano Lett*. **6** 854
[16] Gish D A, Summers M A and Brett M J 2006 *Photon. Nanostruct. Fundam. Appl*. **4** 23
[17] Yang H-Y, Lee M-F, Huang C-H, Lo Y-S, Chen Y-J and Wong M-S 2009 *Thin Solid Films* **518** 1590
[18] Hawkeye M M and Brett M J 2007 *J. Vac. Sci. Technol*. A **25** 1317
[19] Besnard A, Martin N, Carpentier L and Gallas B 2011 *J. Phys. D: Appl. Phys*. **44** 215301
[20] González-García L, Lozano G, Barranco A, Míguez H and González-Elipe A R 2010 *J. Mater. Chem*. **20** 6408
[21] Sánchez-Valencia J R, Toudert J, Borras A, López-Santos C, Barranco A, Ortega-Feliu I and González-Elipe A R 2010 *Plasmonics* **5** 241
[22] Sánchez-Valencia J R, Toudert J, González-García L, González-Elipe A R and Barranco A 2010 *Chem. Comm*. **46** 4372
[23] González-García L, Barranco A, Muñoz-Paez A, González-Elipe A R, García-Gutierrez M C, Hernández J J, Rueda D R, Ezquerra T A and Babonneau D 2010 *Chem. Phys. Chem*. **11** 2205
[24] Nieuwenhuizen J M and Haanstra H B 1966 *Philips Tech. Rev*. **27** 87
[25] Tait R N, Smy T and Brett M J 1993 *Thin Solid Films* **226** 196
[26] Hodgkinson I, Wu Q H and Hazel J 1998 *Appl. Opt*. **37** 2653
[27] Kaminska K, Suzuki M, Kimura K, Taga Y and Robbie K 2004 *J. Appl. Phys*. **95** 3055
[28] Kaminska K, Amassian A, Martinu L and Robbie K 2005 *J. Appl. Phys*. **97** 013511
[29] Buzea C, Beydaghyan G, Elliott C and Robbie K, *Nanotechnology* **16** 1986
[30] Karabacak T, Singh J P, Zhao Y-P, Wang G-C and Lu T-M 2003 *Phys. Rev*. B **68** 125408
[31] Patzig C, Karabacak T, Fuhrmann B and Rauschenbach B 2008 *J. Appl. Phys*. **104** 094318
[32] Ye D-X, Ellison C L, Lim B-K and Lu T-M 2008 *J. Appl. Phys*. **103** 103531
[33] Dirks A G and Leamy H J 1977 *Thin Solid Films* **47** 219
[34] Ye D-X and Lu T-M 2007 Phys. Rev. B **76**, 235402.
[35] Smy T, Vick D, Brett M J, Dew S K, Wu A T, Sit J C and Harris K D 2000 *J. Vac. Sci. Technol*. A **18** 2507
[36] I. Petrov, P.B. Barna, L. Hultman, J.E. Greene, 2003 J. Vac. Sci. Technol. A **21**(5) 117
[37] Borovikov V, Shim Y and Amar J G 2007 *Phys. Rev*. B **76** 241401
[38] Wang S, Xia G, He H, Yi K, Shao J and Fan Z 2007 *J. Alloys Compd*. **431** 287
[39] Lottiaux M, Boulesteix C, Nihoul G, Varnier F, Flory F, Galindo R and Pelletier E. 1989 *Thin Solid Films* **170** 107
[40] Álvarez R, Romero-Gomez P, Gil-Rostra J, Cotrino J, Yubero F, Palmero A and Gonzalez-

Elipe A R 2010 *J. Appl. Phys*. **108** 064316
[41] Álvarez R, Palmero A, Prieto-López L O, Yubero F, Cotrino J, de la Cruz W, Rudolph H, Habraken F H P M and González-Elipe A R 2010 *J. Appl. Phys*. **107** 054311
[42] Hoang V V 2007 *Phys. Stat. Sol*. B **244** 1280
[43] Müller-Pfeiffer S, van Kranenburg H and Lodder J C 1992 *Thin Solid Films* **213** 143
[44] Gupta A, Markworth A J and Saunders J H 1999 *J. Mat. Sci*. **34** 4141
[45] Meunier M, Bernier J-S, Sylvestre J-P and Kabashin A V 2008 *Appl. Surf. Sci*. **254** 2771
[46] Drotar J T, Zhao Y-P, Lu T-M and Wang G-C 2001 *Phys. Rev*. B **64** 125411
[47] Yang H-N, Zhao Y-P, Wang G-C and Lu T-M 1996 *Phys. Rev. Lett*. **76** 3774
[48] Kiema G K, Colgan M J and Brett M J 2005 *Sol. Enery Mater. Sol. Cells* **85** 321

Figure captions:

Figure 1: Schematic description of the deposition process, including a) the deposition chamber, b) the angular distribution of the deposition flux when arriving at the film surface, and c) mechanisms affecting film growth, such as shadowing and nearest-neighbour (NN) sticking: an increasing efficiency of the NN sticking process introduces a vertical growth that reduces the value of the column tilt angle.

Figure 2: Processes included in the Monte Carlo model: a) Head-on collision, with a sticking probability of 1, and b) Nearest-neighbour sticking, with probability s_{nn}. In the top left part of the figure, we show the sticking probability as a function of distance considered in our model.

Figure 3: Comparison of cross-sectional images of experimental (a-d) and simulated (e-h) films, for different values of the incident flux angle, α.

Figure 4: Dependence of column tilt angle, β, on the incident flux angle, α, for experimental and simulated films. Other experimental and theoretical data from the literature have been included.

Figure 5: Dependence of column thickness, ξ, on height, d, obtained from FESEM measurements in figure 3(a-d).

Figure 6: Cross-sectional views of the simulated thin films for $\alpha = 80°$, as a function of s_{nn} and σ.

Figure 7: Simulated column tilt angle, β, as a function of the incident flux angle, α, for different values of s_{nn} and σ. Circles represent results with $\sigma=6°$ and different s_{nn} values, while triangles stand for $s_{nn}=0.12$ and different σ values.

Figure 8: Column thickness, ξ, as a function of height, d, for the simulated films calculated for $\alpha = 80°$, $s_{nn}=0.12$ and different values of σ. The dotted line corresponds to the experimental trend taken from figure 5.

Figure 9: Column thickness, ξ, as a function of height, d, for the simulated films calculated for $\sigma = 6°$, $s_{nn}=0.12$ and different values of α. Dotted lines correspond to the experimental trends taken from figure 5.

Figure 1

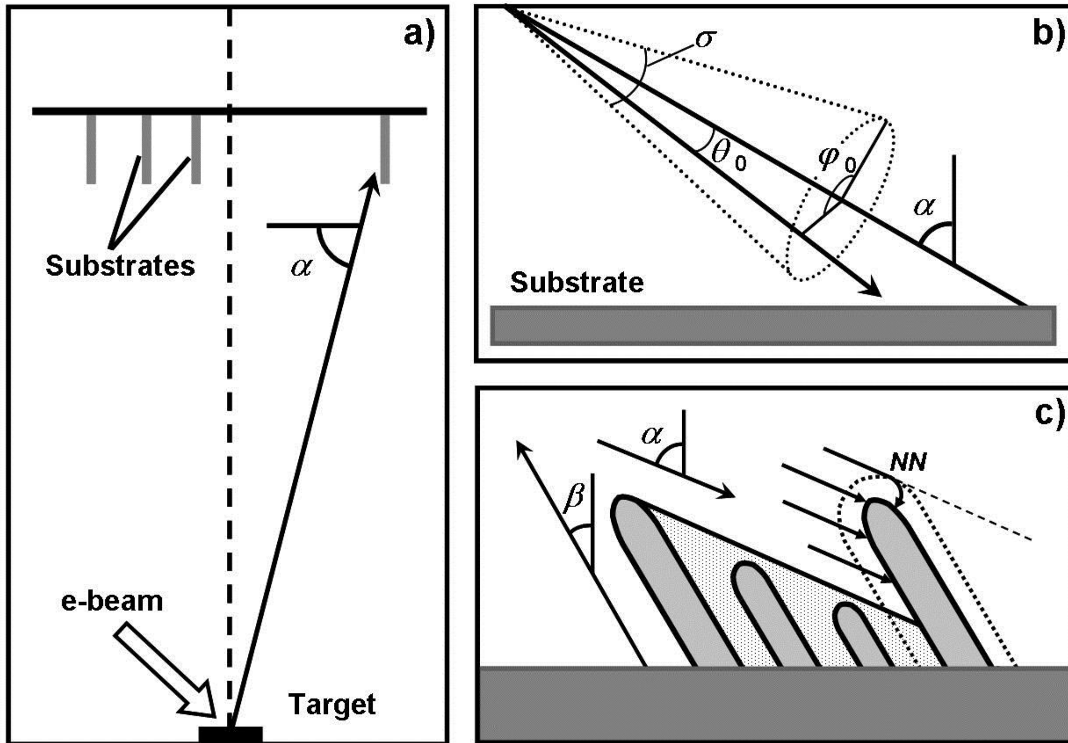

Figure 2

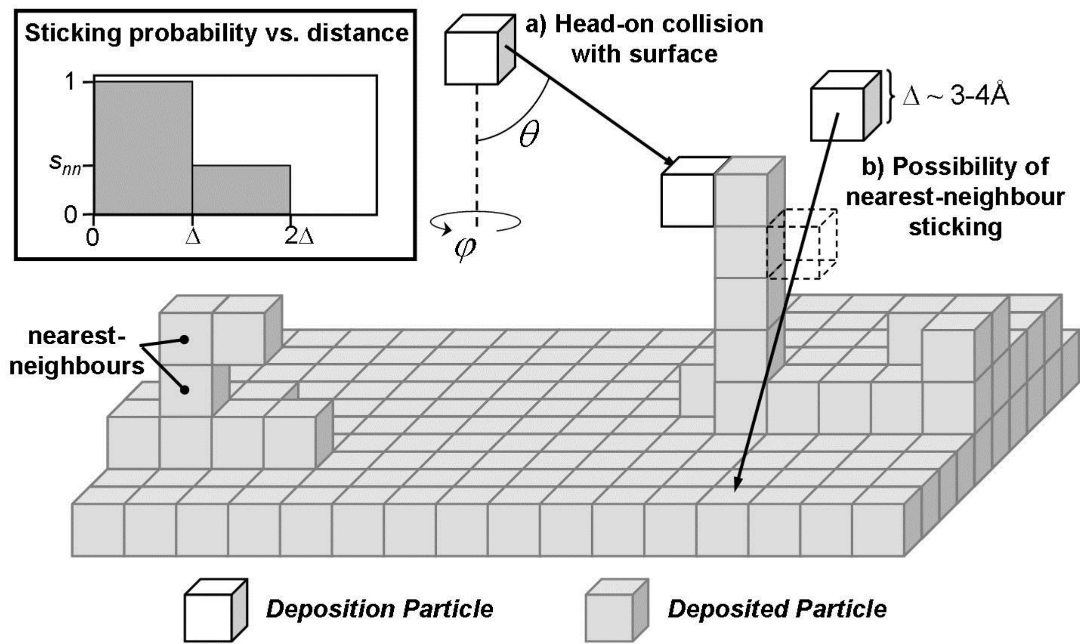

Figure 3

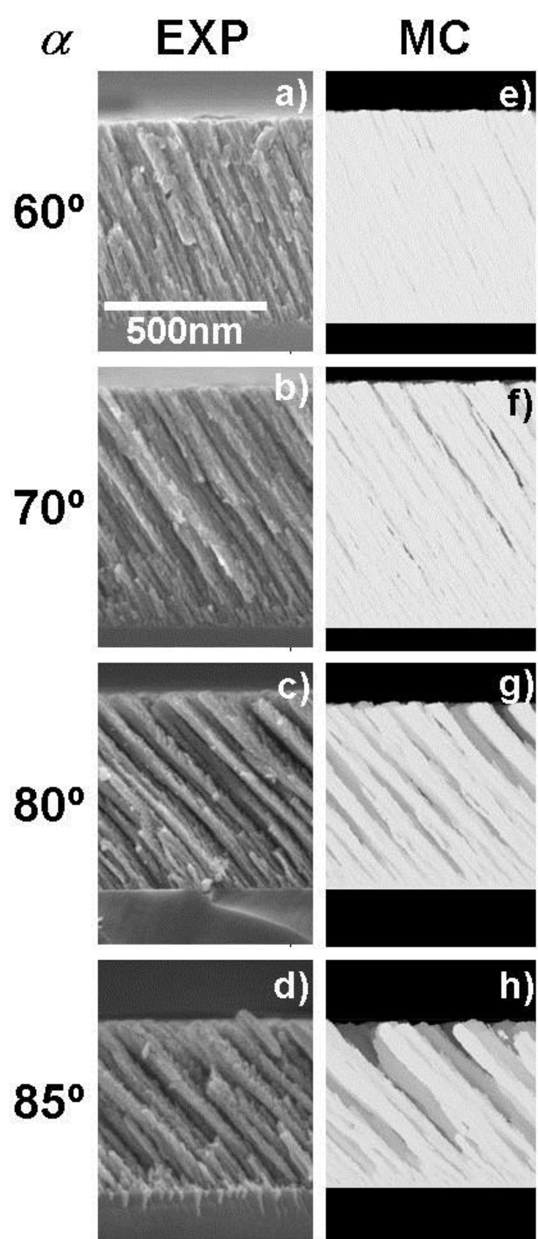

Figure 4

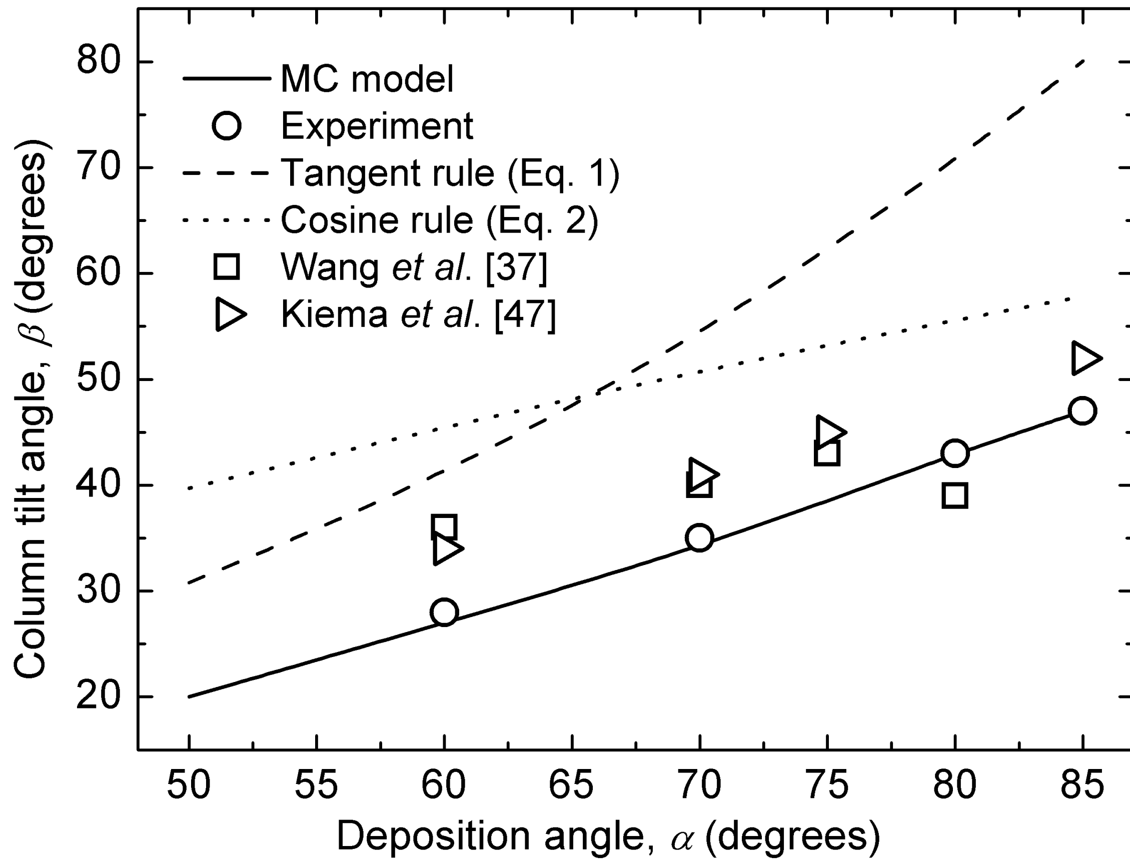

Figure 5

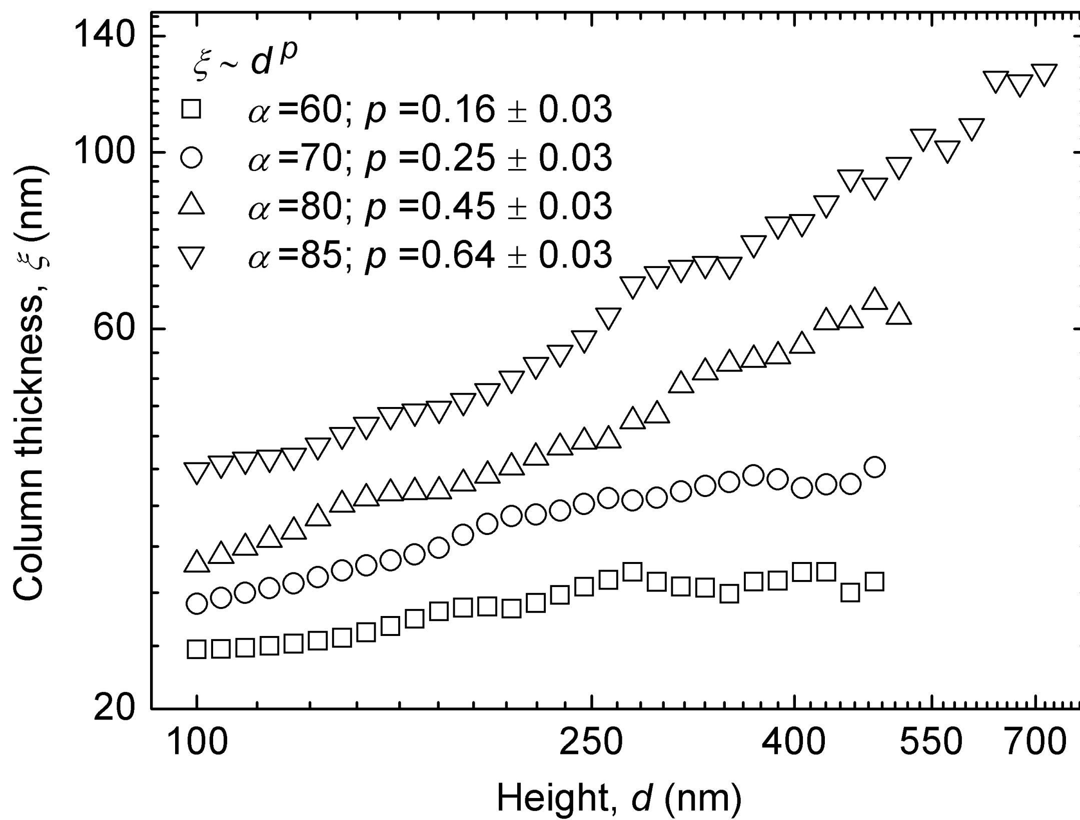

Figure 6

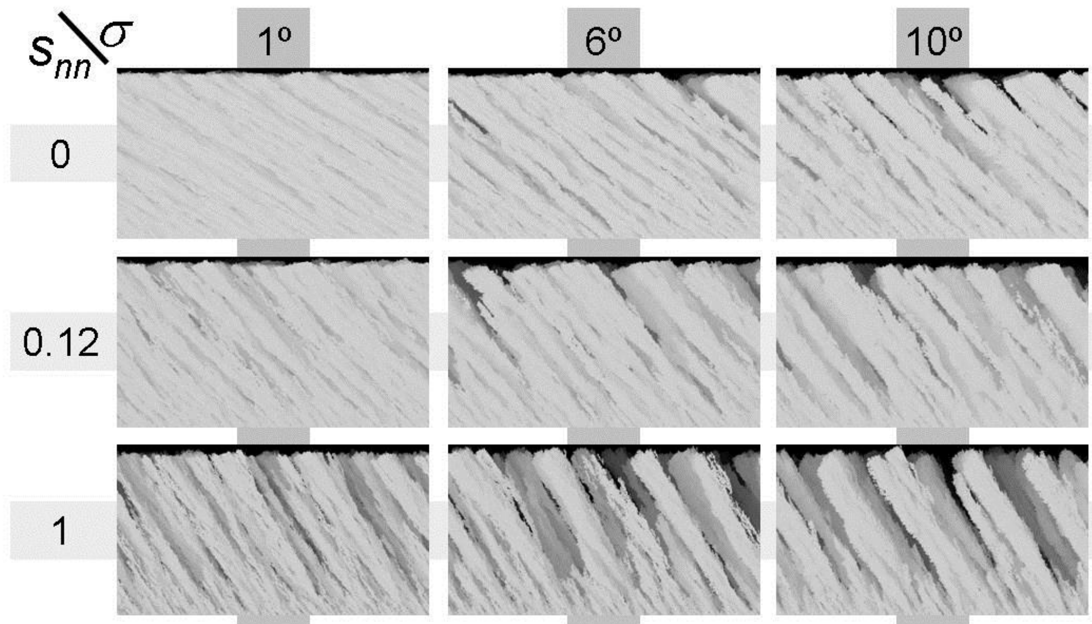

Figure 7

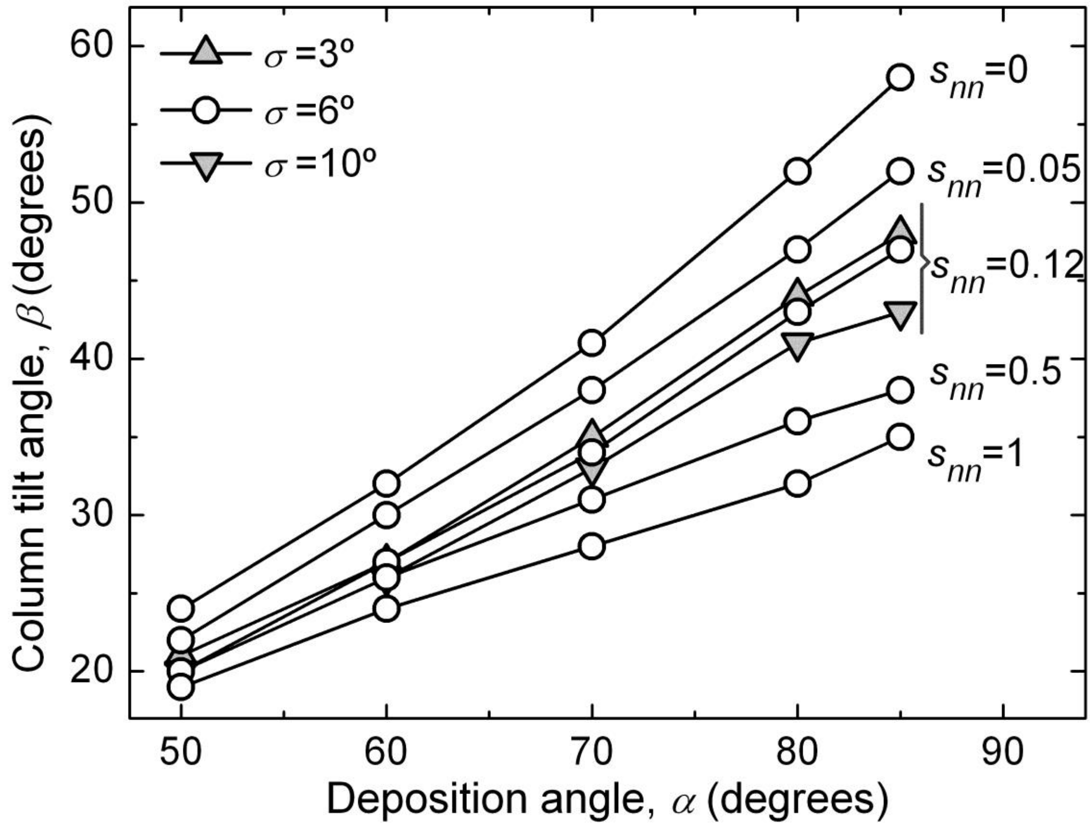

Figure 8

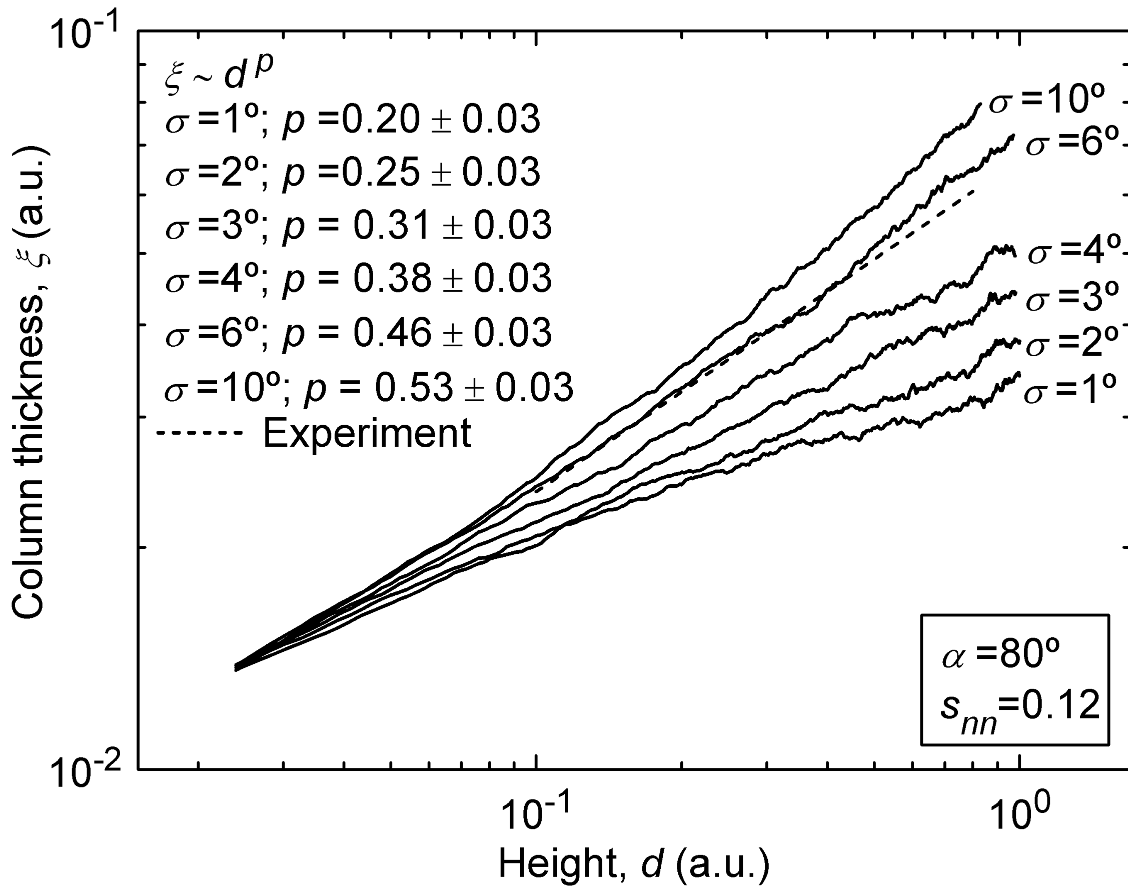

Figure 9